

# Thermal Analysis, Barothermal Treatment, Microstructure, and Properties of an Al–2.5 at % Ca Binary Alloy

A. G. Padalko<sup>a</sup>, \*, M. S. Pyrov<sup>a</sup>, and O. S. Antonova<sup>a</sup>

<sup>a</sup> Baikov Institute of Metallurgy and Materials Science, Russian Academy of Sciences, Moscow, Russia

\*e-mail: padalko@inbox.ru

Received March 21, 2022; revised September 14, 2022; accepted October 11, 2022

**Abstract**—An Al–2.5 at % Ca binary alloy is thermographically studied by differential scanning calorimetry at atmospheric pressure and by differential barothermal analysis at a moderately high argon pressure of ~100 MPa. The baric coefficients of the solidus and liquidus temperatures of the alloy ( $7.5 \times 10^{-2}$  and  $11 \times 10^{-2}$  K/MPa, respectively) exceeding the baric coefficient of the melting temperature of pure aluminum ( $6 \times 10^{-2}$  K/MPa) are found. Barothermal treatment of the alloy is carried out at a subsolidus temperature of 615°C and a pressure of 100 MPa for 180 min. The alloy microstructure is studied. The size distribution of Al<sub>4</sub>Ca intermetallic particles with an average equivalent diameter of ~2.9 μm is established. High porosity of the alloy is revealed. Data on an exponential pore size distribution and on the average pore diameter (~220 nm) are obtained. A model of pore formation as a result of severe generation of dislocations and their subsequent coagulation is proposed. The mechanical properties of the binary alloy are found to be low due to the significant pore density in the material.

**Keywords:** aluminum alloy, differential barothermal analysis, microstructure, porosity, properties

**DOI:** 10.1134/S003602952211009X

## INTRODUCTION

Aluminum-based alloys are under constant active study to improve their technological, mechanical, and performance characteristics. Modifying master alloys were studied for this purpose, and, in the last few years, a conclusion has been drawn that calcium should be used as a promising basic master alloy for complex multicomponent aluminum alloys. The use of calcium as an alloying element is based on the microstructure characteristics of the Al + Al<sub>4</sub>Ca eutectic and the obvious advantage of calcium-containing alloys, such as their low density.

In recent years, cheap, low-density calcium widespread in Earth's crust has been considered as a promising master alloy for light alloys based not only on magnesium [1–5], but also on aluminum. Two intermetallic compounds, Al<sub>4</sub>Ca and Al<sub>2</sub>Ca, form in the Al–Ca binary system. The eutectic with a melting point of 616°C (Fig. 1) forms in the aluminum-rich region in a binary alloy with 5.3 at % (8 wt %) Ca [6, 7]. Three phases identified in the Al–Ca system (aluminum (Al)(Ca) based solid solution; Al<sub>4</sub>Ca, Al<sub>2</sub>Ca compounds) have the following density (g/cm<sup>3</sup>):  $\rho_{\text{Al}} = 2.7$ ,  $\rho_{\text{Al}_4\text{Ca}} = 2.35$ , and  $\rho_{\text{Al}_2\text{Ca}} = 2.42$  [8, 9]. The Al<sub>2</sub>Ca compound melts congruently at 1079°C, and Al<sub>4</sub>Ca forms by the  $L + \text{Al}_2\text{Ca} \rightleftharpoons \text{Al}_4\text{Ca}$  peritectic reaction at 700°C. The Al<sub>4</sub>Ca intermetallic

compound has a volume-centered tetragonal lattice with parameters  $a = 0.436$  nm,  $c = 1.109$  nm, and  $c/a = 2.54$ . The Al<sub>2</sub>Ca compound has the MgCu<sub>2</sub> structure with a lattice parameter  $a = 0.8038$  nm [6].

Studies on aluminum-based calcium-containing binary alloys included equiaxed angular pressing of the Al–8 at % Ca alloy [10, 11]. These studies report a high dislocation density and the formation of a nanodispersed crystalline structure with typical crystalline

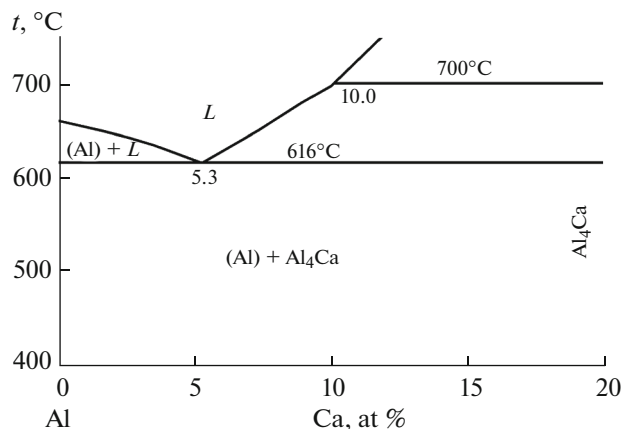


**Fig. 1.** Fragment of the Al–Ca phase diagram.

sizes of 25–45 nm. A further study of calcium-containing aluminum alloys was carried out on multicomponent materials containing 2–10 wt % Ca [12–17]. Al–Ca–Ni–Sc alloys were synthesized and investigated. The advantages of these alloys include the necessity of heat treatment without quenching.

There are no works on hot isostatic pressing of both binary and multicomponent aluminum alloys among works on the synthesis of calcium-containing aluminum alloys and studying their properties. However, the widespread use of this technique in metal science gives reason to believe that barothermal treatment of aluminocalcium alloys may be appropriate to remove porosity, to influence the structural components and, ultimately, the physical and mechanical properties of this promising group of aluminum materials [18]. This work aims to study the static barothermal effect on an Al–2.5 at % Ca binary alloy.

## EXPERIMENTAL

The Al–2.5 at % Ca alloy was synthesized by melting from the initial metals in aluminum crucibles. Samples 20 mm in diameter and 120 mm in length were cast in cylindrical graphite–fireclay molds. Barothermal treatment (BTT) and differential barothermal analysis (DBA) were carried out on an ABRA HIRP 25/70–200–2000 isostatic press (Switzerland) using graphite heaters made of a carbon–carbon composite material. The starting pressure of argon in the high-pressure vessel (HPV) in both the BTT and DBA cycles was ~51 MPa. The system of linear temperature increase was actuated. At the final stage of heating, the pressure in the HPV was ~100 MPa. The holding time of the samples ranged from 5 (DBA) to 180 min (BTT), depending on the task of the cycle performed. Subsequently, the temperature was linearly reduced to ~300°C and then to room temperature using a rapid cooling system. The castings were then taken out to prepare samples for analysis.

Billets to be ground were cut on a Struers Discotom machine. The surface for the analysis was prepared on a TF 250 grinding and polishing machine (Germany) using diamond pastes, gradually reducing the grain size of the pastes. Chemical etching was not performed. Vickers microhardness was measured on a LOMO PMT-3M tester at a load of 0.5 N (50 gf) for 15 s. X-ray diffraction analysis (XRD) of the powder samples was carried out on a DRON-3 diffractometer using  $\text{CuK}\alpha_1$  radiation at a wavelength of 1.5406 Å and a step of  $\Delta 2\theta = 0.02^\circ$  in the range  $31^\circ \leq 2\theta \leq 96^\circ$ . Differential scanning calorimetry (DSC) of samples 5 mm in diameter and 1 mm thick at atmospheric pressure was performed using a Netzsch STA 449F1 Jupiter unit (Germany) in an argon stream at heating/cooling rates of 7 K/min. These results were used as reference ones. Differential barothermal analysis was carried out at a melting temperature of the binary alloy using a differential thermal analysis (DTA) cell

located in an HPV isostatic press in an argon atmosphere compressed to ~100 MPa. Optical microscopic images (OM) were taken at a magnification of  $\times 1500$  using a Leica DM 6M metallographic system (Germany). High-resolution images and the results of elemental analysis were taken using a Vega Tescan 3 scanning electron microscope (SEM, Germany).

## RESULTS AND DISCUSSION

The study of the microstructure of the synthesized alloy showed that the material consisted of primary aluminum dendrites with first order axis dimensions of about 30–100  $\mu\text{m}$  and Al +  $\text{Al}_4\text{Ca}$  eutectic in the interdendritic spaces, where intermetallic particles were about a micrometer in size (Fig. 2).

The DSC was carried out at atmospheric pressure to obtain reference data on phase transformations in the Al–2.5 at % Ca alloy (Figs. 3a, 3b). This experiment revealed practical coincidence between the solidus and liquidus temperatures of the alloy and the literature data [6] (616 and 615°C solidus temperature, 641 and 642°C liquidus temperature according to the literature data and DSC results, respectively). Analysis of the DSC curve in the low-temperature range  $240 \leq t \leq 450^\circ\text{C}$  (Fig. 3b) showed small thermal effects I, II and III, corresponding to the beginning of transformations at 241, 303, and 334°C. These effects can be attributed to the simultaneous processes of coagulation (exothermic) and dissolution (endothermic) of  $\text{Al}_4\text{Ca}$  particles. One or another process dominates depending on the temperature, resulting in a pulsating character of the total heat effect registered by the DSC apparatus. A similar result was obtained in the thermographic study of a compacted and extruded calcium–aluminum metal mixture (Fig. 3c) [19]. Resulting thermal effects I and II, which began at 272 and 317°C, were associated with the beginning of the interaction between metallic aluminum and calcium and the formation of  $\text{Al}_4\text{Ca}$  and  $\text{Al}_2\text{Ca}$  intermetallic compounds, which becomes possible at relatively low temperatures and correlates with the DSC results for the Al–2.5 at % Ca alloy at atmospheric pressure.

To detect possible phase transformations and baric shift in the characteristic temperatures, the differential thermal analysis at high pressure (DBA) of the alloy was carried out in the pressure range 50–114 MPa (Fig. 3d). Weak thermal effects corresponding to the dissolution and coagulation processes of fine  $\text{Al}_4\text{Ca}$  particles were recorded on heating curve 1. Dissolution with an endoeffect began at 198°C and a pressure of 67 MPa. At a pressure of 76 MPa, the exothermic effect of coagulation slightly exceeded the endothermic effect of dissolution starting from 318°C. Coagulation prevailed in the material starting from 370°C and a pressure of 84 MPa. We should note that insolubility of calcium in the aluminum matrix under normal conditions [6] can be overcome by the thermody-

namically driven dissolution process of  $\text{Al}_4\text{Ca}$  in aluminum to form a solid solution with a density close to the aluminum density, which is favorable for the system under moderately high all-round pressure. The solidus temperature of the alloy (eutectic temperature) at 107 MPa increased to 623°C (at canonical data 616°C). During further heating the liquidus temperature was fixed at 653°C and a pressure of 110 MPa. The beginning of crystallization at 653°C on the cooling curve 2 (Fig. 3d) coincides with the liquidus temperature on the heating curve 1. This fact can be explained by a lack of melt supercooling during the formation of critical-sized nuclei at high pressure; i.e., nucleation in the alloy at moderately high pressure occurs by a homogeneous mechanism. The eutectic solidification temperature in this experiment was 612°C ( $\Delta t = -4^\circ\text{C}$ ). A weak exothermic effect with the beginning at 542°C was observed in the solid phase during cooling, which is most likely associated with the coagulation of fine  $\text{Al}_4\text{Ca}$  particles formed during alloy solidification.

The baric coefficients of the solidus and liquidus temperatures were  $7.5 \times 10^{-2}$  and  $11 \times 10^{-2}$  K/MPa, respectively, which are significantly higher than the baric coefficient of melting temperature of pure aluminum ( $6 \times 10^{-2}$  K/MPa), whose specific volume grows less during melting than that for the Al–2.5 at % Ca binary alloy. The DBA results are shown in the fragment of the Al–Ca phase diagram (Fig. 4).

The detected baric increase in the solidus temperature of the alloy provides the possibility of BTT of the alloy at elevated temperatures. The implemented BTT temperature was 615°C, which practically coincides with the solidus temperature of the alloy under normal conditions. The castings were placed in the same working volume as the DBA cell during this experiment. For thermal analysis, alloy samples 4 mm in diameter and 7 mm in height were prepared; pure aluminum was used as a reference. Figure 5 shows the temperature of the sample and the massive castings as a function of the holding time, as well as the change in the differential signal over time. An endothermic effect starting at 327°C and 73 MPa was detected on the differential curve during heating, which correlates with the DBA results. The treatment was performed by linear heating at a rate of 5 K/min, holding at 615°C and a pressure of 102 MPa for 180 min, as well as linear cooling at the same rate. The exothermic effect was fixed immediately after the beginning of cooling. It is probably related to the parallel processes of (Al)⟨Ca⟩ solid solution decomposition and coagulation of  $\text{Al}_4\text{Ca}$  microparticles formed during solidification.

Two structural constituents were detected in the alloy microstructure after the BTT (Fig. 6), namely, primary aluminum dendrites and  $\text{Al}_4\text{Ca}$  particles significantly increased in comparison with those in the initial alloy. Statistical analysis showed that the average equivalent diameter of microparticles was  $\sim 2.9 \mu\text{m}$  (Fig. 7), which was comparable with that of the silicon

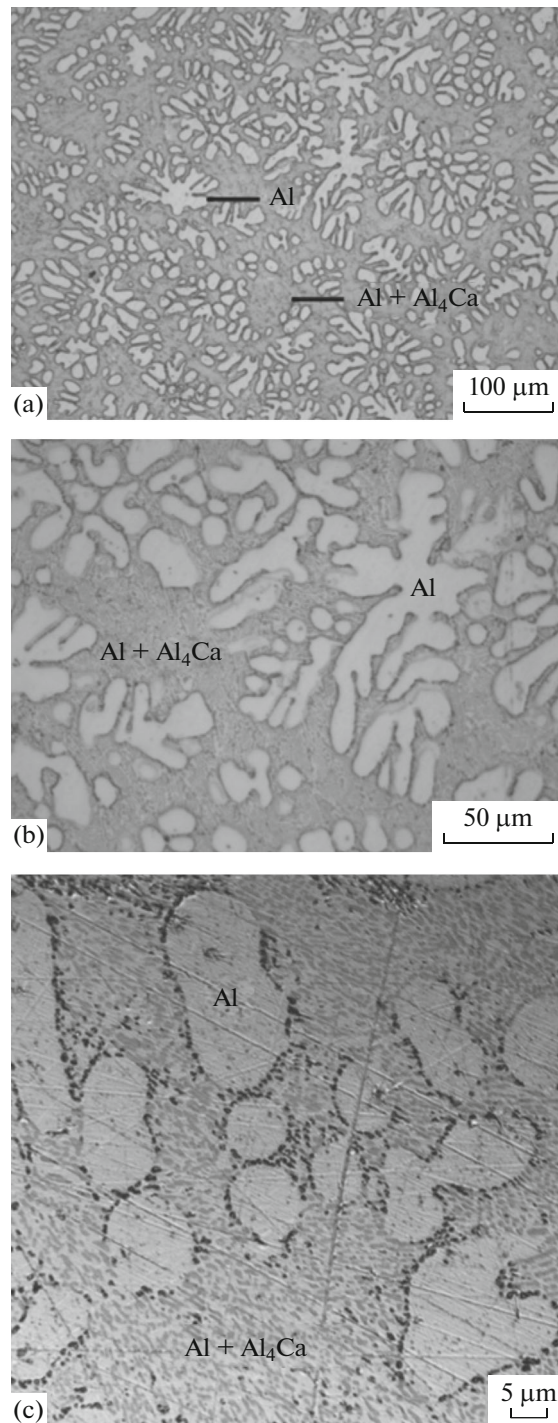
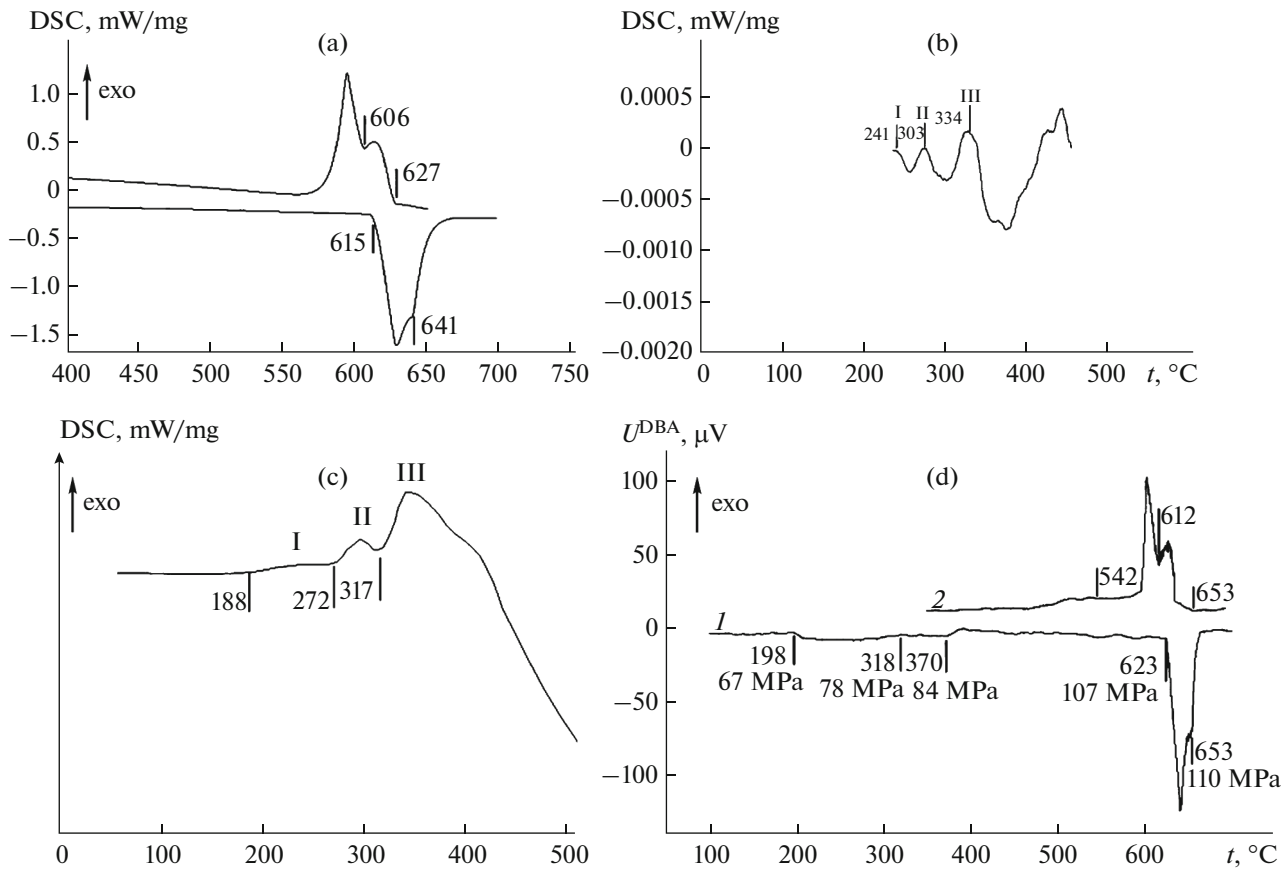


Fig. 2. Microstructure (OM) of the initial Al–2.5 at % Ca binary alloy: (a)  $\times 200$ , (b)  $\times 500$ , and (c)  $\times 1500$ .

particles in the Al–8 at % Si binary alloy [20]. When the morphology of the particles was sufficiently compact, the degree of roundness was determined by the expression

$$C = 4\pi A^2 / P^2, \quad (1)$$



**Fig. 3.** Thermography of the Al–2.5 at % Ca alloy: (a) DTA curves at atmospheric pressure, (b) low-temperature fragment of the DTA heating curve with increased resolution along the ordinate axis of the curve in (a) with thermal effects I, II and III of  $Al_4Ca$  particle coagulation, (c) DTA heating curve at atmospheric pressure [19], and (d) (1) heating and (2) cooling curves of DBA alloy in the pressure range 50–114 MPa.

where  $A$  is the particle area and  $P$  is the perimeter of the particle.

According to Eq. (1), roundness  $C$  of a regular circle is equal to one and decreases as the ratio of particle

length to its width increases. The processing of the OM image resulted in a histogram of particle number distribution depending on their roundness (Fig. 8). In this distribution the maximum number of particles falls on a roundness of  $\sim 0.37$  at its minimum value of

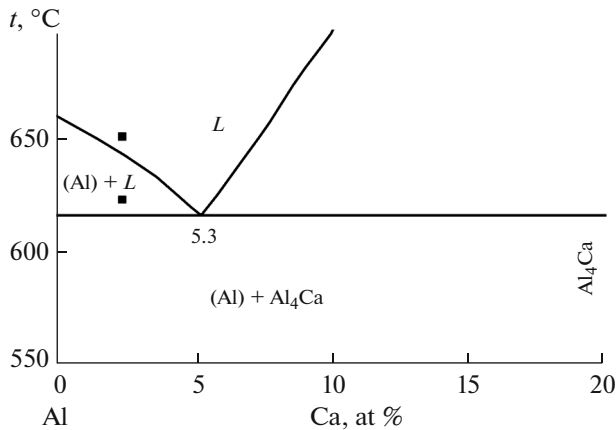


**Fig. 4.** Fragment of the Al–Ca phase diagram [7] with experimental points of solidus and liquidus temperatures obtained by DBA of Al–2.5 at % Ca alloy at a pressure of  $\sim 100$  MPa.

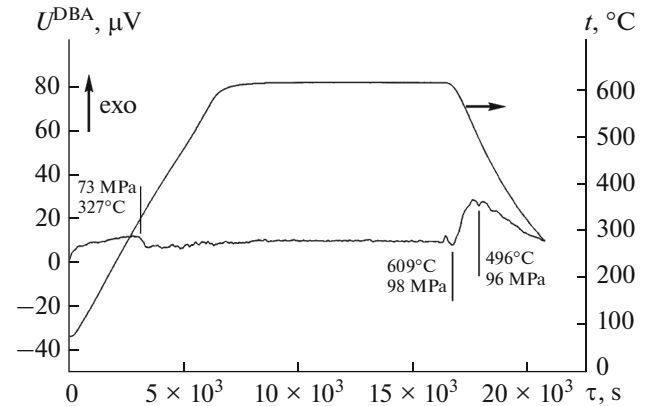


**Fig. 5.** BTT cyclogram of Al–2.5 at % Ca alloy with the DBA curve taken during the combined BTT and DBA process at a heating/cooling rate of 5 K/min.

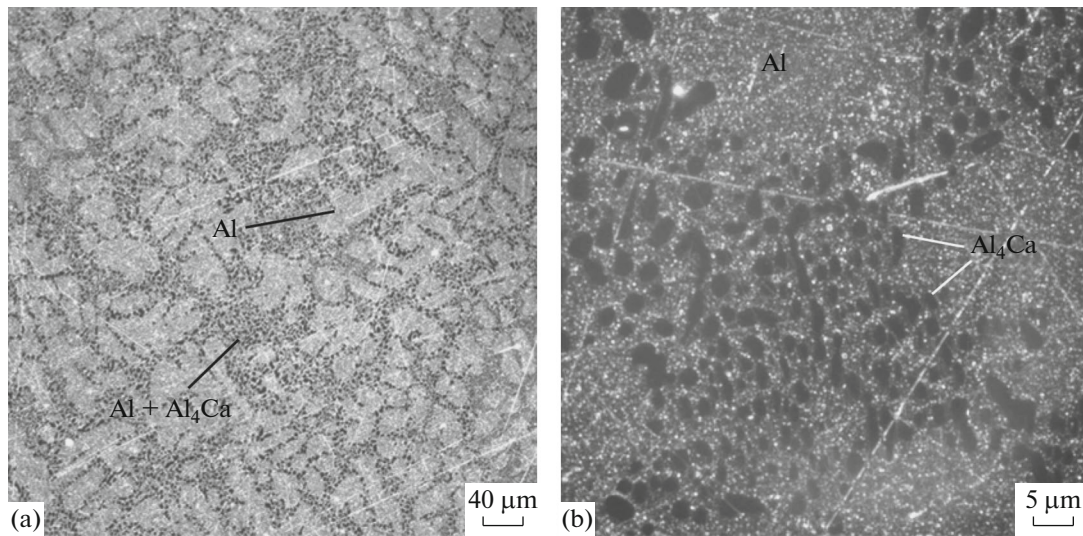


**Fig. 6.** OM dark-field images of the microstructures of the Al–2.5 at % Ca alloy after BTT performed at 100 MPa and 615°C for 3 h.

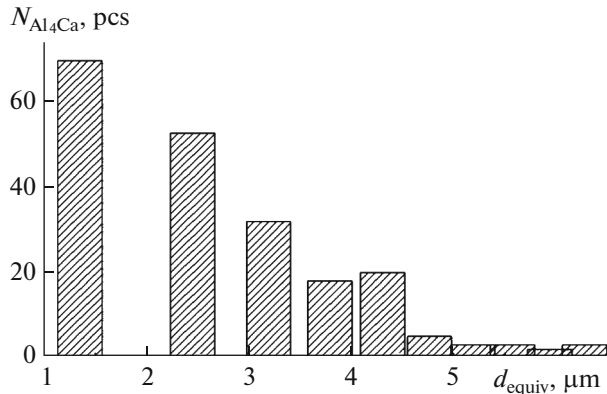


**Fig. 7.** Size distribution of Al<sub>4</sub>Ca particles in the Al–2.5 at % Ca alloy after BTT performed at 100 MPa and 615°C for 3 h.

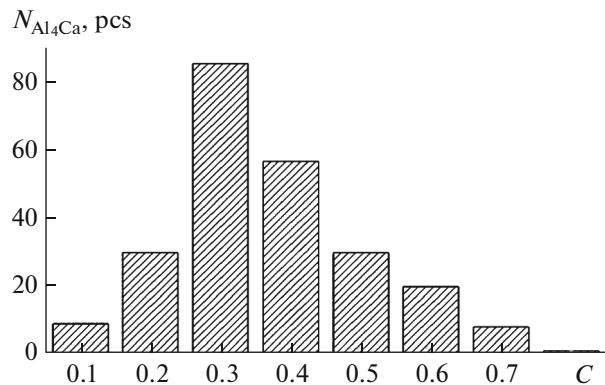


**Fig. 8.** Roundness ( $C$ ) distribution of Al<sub>4</sub>Ca particles in the Al–2.5 at % Ca alloy after BTT.

$C \approx 0.1$ . The large number of particles has a roundness of up to  $\sim 0.8$  and the average roundness is  $0.37 \pm 0.14$ , which indicates a high degree of spheroidization of intermetallic particles.

The phase composition was determined by XRD of a mechanically ground powder sample (Fig. 9). To determine the lattice parameters of aluminum and Al<sub>4</sub>Ca, silicon powder was added to the alloy powder as a reference substance. The reflection of Al and Al<sub>4</sub>Ca with possible small content of Al<sub>2</sub>Ca was identified on the X-ray diffraction pattern in the range  $30^\circ \leq 2\theta \leq 96^\circ$ . In the latter case, the results should be clarified due to the small amounts of this component and the overlapping of diffraction peaks.

Further study of the chemical composition of the alloy was carried out using electron-probe microanalysis (EPMA). Therefore, we analyzed the chemical

composition of aluminum dendrites and Al<sub>4</sub>Ca particles in the interdendritic spaces (Fig. 10).

The dendrites of the Al matrix were found not to contain calcium, which corresponds to the idea of low solubility of calcium in aluminum. However, the chemical composition of the Al<sub>4</sub>Ca particles significantly differs from the stoichiometric composition of the Al<sub>4</sub>Ca compound (Table 1). The aluminum and cal-

**Table 1.** EPMA results for two Al<sub>4</sub>Ca particles (Fig. 10b)

Oe	Spectrum 1	Spectrum 3
	at %	
O <i>K</i>	4.87	0.05
Al <i>K</i>	87.23	82.19
Ca <i>K</i>	7.90	7.76

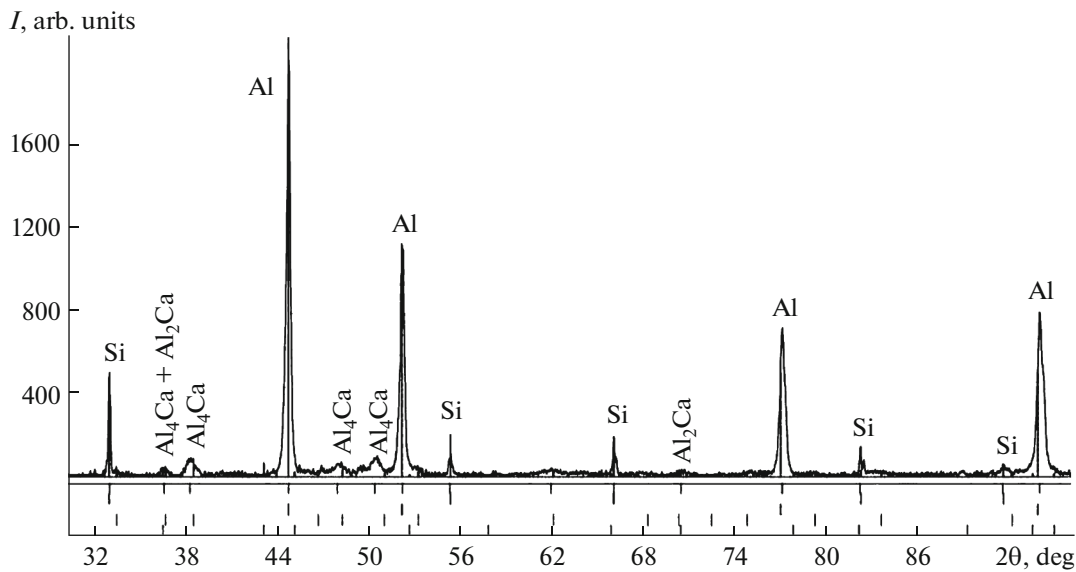


**Fig. 9.** XRD pattern of the powder Al–2.5 at % Ca alloy sample with addition of reference silicon powder after BTT performed at 100 MPa and 615°C for 3 h.

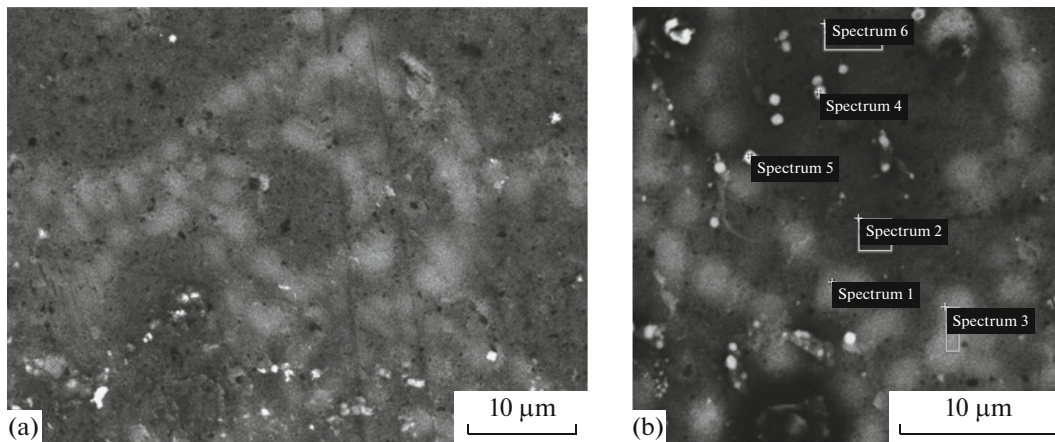


**Fig. 10.** (a) SEM image of  $\text{Al}_4\text{Ca}$  particles and aluminum matrix and (b) typical EPMA data.

cium content according to two available spectra varied between 82.2–87.2 at % Al and 7.8–7.9 at % Ca, whereas if the composition corresponds to the chemical formula the aluminum content should not exceed 46.8 at %. The resulted data on calcium content are most likely to be determined by the small size of the intermetallic particles and by the formation of the output signal from both the intermetallic particles and the aluminum matrix.

SEM showed a high pore density in the aluminum matrix of the alloy after BTE (Fig. 11a). The pore size distribution was obtained by tool processing of an image (Fig. 11b) and subsequent statistical processing (Fig. 11c). The distribution is satisfactorily approxi-

mated by the expression  $N_n = 3.2 \times 10^2 \exp(-0.01d_n)$ , where  $d_n$  is the equivalent diameter (nm) at an average equivalent diameter of ~200 nm. The porosity of the aluminum matrix in this case reached 6–7 vol %. This fact can be explained by the high BTT temperature, which almost coincides with the solidus temperature of the alloy under normal conditions, and an applied all-round pressure of ~100 MPa. At these parameters, an active generation of dislocations occurs in the aluminum matrix, and they then coagulate with the formation of pores.

A high dislocation density was also observed in the Al–16 at % Si binary alloy after the BTT at 560°C, 100 MPa, and 3 h [20, 21], i.e., at a temperature by

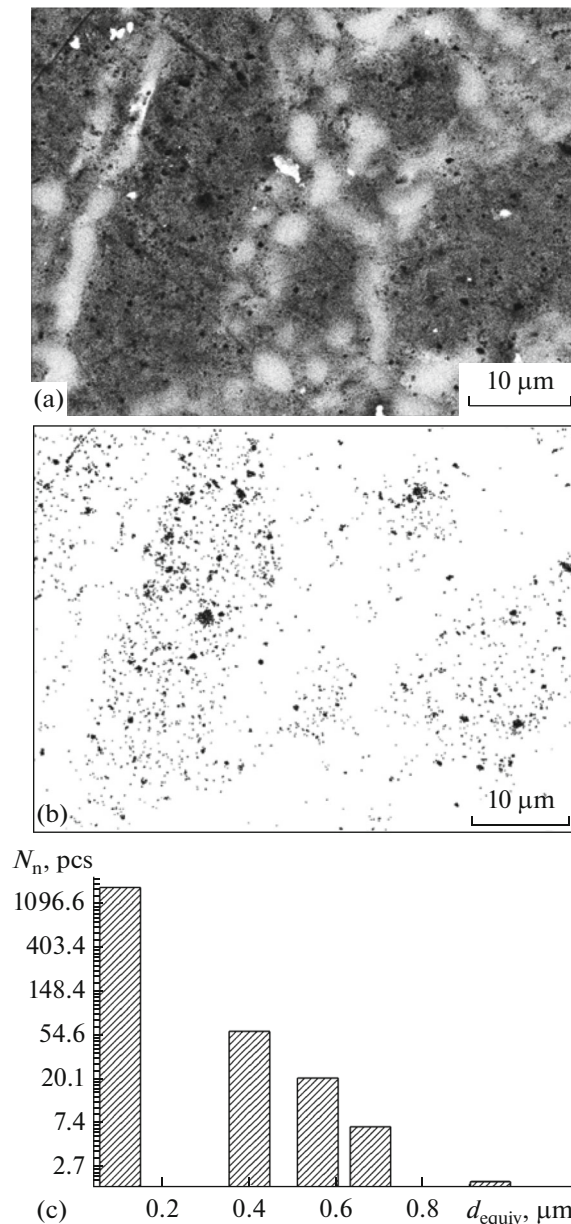


**Fig. 11.** Pores in the aluminum matrix of the Al–2.5 at % Ca alloy after BTT: (a) SEM image, (b) image processed for the statistical processing, and (c) histogram of pore size distribution.

55°C lower than that of the Al–2.5 at % Ca alloy. In the latter case, the intensity of dislocation generation may significantly increase and result in their further coagulation. The possible involvement of calcium vapor in the pore-forming process seems unlikely, since at 1103 K the saturated vapor pressure in the calcium triple point is 0.37 kPa [22], which is many times lower than the applied external pressure. The homogeneous distribution of pores in the aluminum matrix, regardless of the distance from the sample surface, indicates that pore formation due to argon diffusion also cannot cause their formation.

Samples for uniaxial tension tests were prepared from the barothermally treated alloy (Fig. 12a). Figure 12b shows a typical experimental dependence  $\sigma = f(\delta)$  for the Al–2.5 at % Ca binary alloy after a BTT performed at 100 MPa and 615°C for 3 h.

The test results for the three samples are shown in Table 2. According to the given data the alloy has low strength characteristics: a yield strength of  $80.3 \pm 3.1$  MPa, an ultimate tensile strength of  $110.5 \pm 7.7$  MPa, and a relative elongation of  $6.3 \pm 6\%$ . The developed porosity of the samples is a determining factor for crack nucleation in the material and, as a

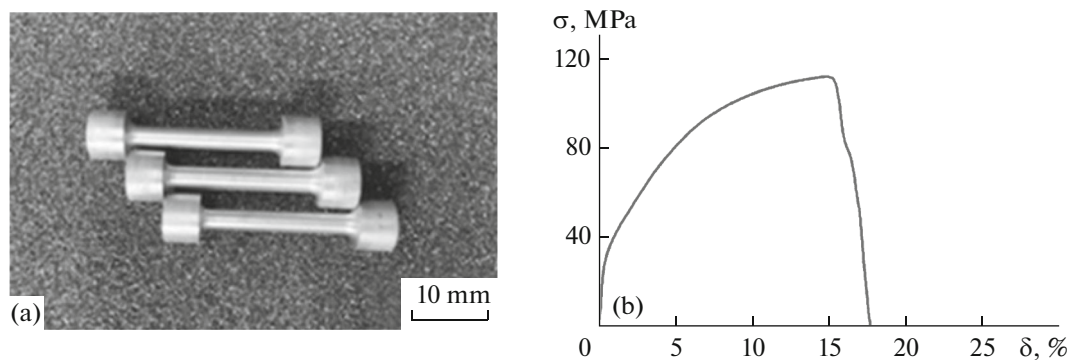


Fig. 12. (a) Samples for uniaxial tension tests and (b) experimental dependence  $\sigma = f(\delta)$ .

consequence, a possible decrease in the mechanical properties of the barothermally treated Al–2.5 at % Ca binary alloy.

## CONCLUSIONS

(1) The Al–2.5 at % Ca binary alloy was thermographically studied by DSC at atmospheric pressure and by DBA at a moderately high argon pressure of  $\sim 100$  MPa. The baric coefficients of the solidus and liquidus temperatures of the alloy were found to be  $7.5 \times 10^{-2}$  and  $11 \times 10^{-2}$  K/MPa, respectively. They are higher than the baric coefficient of the melting temperature of pure aluminum ( $6 \times 10^{-2}$  K/MPa).

(2) BTT of the alloy was carried out at a subsolidus temperature of  $615^\circ\text{C}$  and a pressure of 100 MPa for 180 min. The alloy microstructure was studied. The size distribution of  $\text{Al}_4\text{Ca}$  intermetallic particles with an average equivalent diameter of  $\sim 2.9 \mu\text{m}$  was established.

(3) The alloy structure was found to have a high degree of porosity. Exponential pore-size distribution and an average pore diameter of  $\sim 220$  nm were found.

(4) A model of pore formation due to the active generation of dislocations and their subsequent coagulation was proposed. The mechanical properties of

the binary alloy were found to be low due to a significant pore density in the material.

## CONFLICT OF INTEREST

The authors declare that they have no conflicts of interest.

## REFERENCES

- S. Gneiger, N. Papenberg, A. Arnoldt, C. M. Schlögl, and M. Fehlbier, "Investigations of high-strength Mg–Al–Ca–Mn alloys with a broad range of Ca + Al contents," *Materials* **14** (18), 5439 (2021). <https://doi.org/10.3390/ma14185439>
- F. Guo, B. Feng, S. Fu, Y. Xin, S. Xu, and Q. Liu, "Microstructure and texture in an extruded Mg–Al–Ca–Mn flat-oval tube," *J. Magnes. Alloys* **5** 13–19 (2017).
- J. Li, A. Zhang, H. Pan, Y. Ren, Z. Zeng, Q. Huang, C. Yang, L. Ma, and G. Qin, "Effect of extrusion speed on microstructure and mechanical properties of the Mg–Ca binary alloy," *J. Magnes. Alloys* **9** (4) (2020). <https://doi.org/10.1016/j.jma.2020.05.011>
- H. Pan, R. Kang, J. Li, Z. Zhuoran, H. Xie, Q. Huang, C. Yang, Y. Ren, and G. Qin, "Mechanistic investigation of a low-alloy MgCa-based extrusion alloy with high strength-ductility synergy," *Acta Mater.* **186**, 7652 (2020). <https://doi.org/10.1016/j.actamat.2020.01.017>
- D. Makwana and P. Bhingole, "Effects of Ca and Al on microstructural and tribological behavior of Mg–Al–Ca ternary alloy," *Mater. Today* (2020). <https://doi.org/10.1016/j.matpr.2020.02.425>
- Phase Diagrams of Binary Metallic Systems: A Handbook*, Ed. by Lyakishev (Mashinostroenie, Moscow, 1996), Vol. 1.
- N. A. Belov, E. A. Naumova, and T. K. Akopyan, *Eutectic Alloys Based on Aluminum: New Systems and Alloying* (Ruda Metally, Moscow, 2016).
- N. A. Belov, A. A. Aksenov, and D. G. Eskin *Iron in Aluminium Alloys* (Taylor Francis, London, 2002).
- "Pauling file" in *Inorganic Solid Phases Springer Materials (online database)*, Ed. by P. Villars (Springer, Heidelberg, 2016).

Table 2. Mechanical properties of Al–2.5 at % Ca binary alloy after BTT performed at 100 MPa and  $615^\circ\text{C}$  for 3 h

Sample	$\sigma_{0.2}$	$\sigma_u$	$\delta, \%$
	MPa		
1	78.2	102.16	1.2
2	78.4	117.42	13.2
3	84.4	111.97	5.98
Average	$80.3 \pm 3.5$	$110.5 \pm 7.7$	$6.34 \pm 6.0$

$\sigma_{0.2}$  is the yield strength,  $\sigma_u$  is the ultimate tensile strength, and  $\delta$  is the relative elongation.



10. S. O. Rogachev, E. A. Naumova, E. S. Vasileva, and R. V. Sundeev, "Al–Ca, Al–Ce, and Al–La eutectic aluminum alloys processed by high-pressure torsion," *Advanc. Eng. Mater.* **24** (2), 2100772 (2021).  
<https://doi.org/10.1002/adem.202100772>
11. S. O. Rogachev and E. A. Naumova, "Thermal stability of Al–Ca and Al–Ce alloys obtained by high-pressure torsion," *J. Mater. Eng. Perform.* **30**, 9192–9199 (2021).  
<https://doi.org/10.1007/s11665-021-06105-4>
12. E. Naumova, V. Doroshenko, M. Barykin, T. Sviridova, A. Lyasnikova, and P. Shurkin, "Hypereutectic Al–Ca–Mn–(Ni) alloys as natural eutectic composites," *Metals* **11** (6), 890 (2021).  
<https://doi.org/10.3390/met11060890>
13. N. A. Belov, E. A. Naumova, T. K. Akopyan, and V. V. Doroshenko, "Design of multicomponent aluminium alloy containing 2 wt % Ca and 0.1 wt % Sc for wrought and cast products," *J. Alloys Compd.* **762**, 528–536 (2018).
14. E. A. Naumova, "Use of calcium in alloys: from modifying to alloying," *Russ. J. NonFerr. Met.* **59**, 284–298 (2018).
15. N. A. Belov, E. A. Naumova, T. A. Bazlova, and V. V. Doroshenko, "Phase composition and hardening of castable Al–Ca–Ni–Sc alloys containing 0.3% Sc," *Met. Sci. Heat Treat.* **59**, 76–81 (2017).
16. N. A. Belov, E. A. Naumova, V. V. Doroshenko, and T. A. Bazlova, "Effect of manganese and iron on the phase composition and microstructure of aluminum-calcium alloys," *Tsvet. Met.* **8**, 66–71 (2017).
17. S. O. Rogachev, E. A. Naumova, R. V. Sundeev, and N. Y. Tabachkova, "Structural and phase transformations in a new eutectic Al–Ca–Mn–Fe–Zr–Sc alloy induced by high pressure torsion," *Mater. Lett.* **243**, 161–164 (2019).
18. V. V. Doroshenko, "Manufacturability of multicomponent aluminum–calcium alloys during casting and pressure treatment," *Cand. Sci. (Eng.) Dissertation*, MISiS, Moscow, 2019.
19. L. Tian, H. Kim, I. Anderson, and A. Russell, "The microstructure-strength relationship in a deformation processed Al–Ca composite," *Mater. Sci. Eng. A* **570**, 106–113 (2013).
20. A. G. Padalko, M. S. Pyrov, R. D. Karelin, V. S. Yusupov, and G. V. Talanova, "Barothermal treatment, cold plastic deformation, microstructure and properties of binary silumin Al–8 at % Si," *Russ. Metall. (Metally)*, No. 9, 1155–1164 (2021).
21. E. V. Dedyeva, A. G. Padalko, D. V. Zaitsev, E. A. Lukina, P. N. Nikiforov, G. V. Talanova, and K. A. Solntsev, "Effect of barothermal processing on the solid-state formation of the structure and properties of 16 at % Si–Al hypereutectic alloy," *Inorg. Mater.* **54** (2), 125–132 (2018).  
<https://doi.org/10.1134/S0020168518020024>
22. V. M. Azhazha, P. N. V'yugov, V. B. Kryukov, and G. F. Tikhinskii, "Production of high-purity calcium and study of some of its properties," *Vopr. At. Nauki Tekh., Ser. Fiz. Radiats. Povrezhdenii Radiats. Materialoved.*, Nos. 2 (62)/3 (63), 129–132 (1994).

*Translated by T. Gapontseva*